

## Theoretical and Experimental Investigation of Interferometric Absorbers for Thermal Infrared Detectors

Pontus Eriksson, Jan Y. Andersson<sup>1</sup> and Göran Stemme

Instrumentation Laboratory, Royal Institute of Technology (KTH), S-100 44 Stockholm, Sweden

<sup>1</sup>Industrial Microelectronics Center (IMC), P. O. Box 1084, S-164 21 Kista, Sweden

(Received November 30, 1995; accepted August 6, 1996)

**Key words:** interferometric absorber, air gap, silicide, FTIR, surface micromachining

One of the most essential parts of a thermal IR detector is the absorber which is expected to provide a high absorptance in the specified wavelength range without adding too much thermal mass. An absorber which satisfies these requirements is an interferometric structure which consists of a reflector, an air gap of thickness approximately equal to a quarter wavelength, a thin resistive absorbing film with sheet resistance close to  $377 \text{ } (\Omega/\text{square})$  (the vacuum characteristic impedance), and a thin dielectric film needed for mechanical support of the latter. Such absorbers were fabricated and characterized and their spectra were compared with theoretically simulated spectra. The fabrication was based on surface micromachining with silicon nitride as the dielectric medium, and gold as the reflector. Sputter-deposited molybdenum silicide was, for the first time, tested as the resistive absorbing film. Polyimide was used as a sacrificial layer during membrane fabrication. The samples were characterized using Fourier transform infrared spectroscopy. After compensation for a nonunity fill factor, a mean absorptance of 80–90% was obtained in the very broad wavelength region of 8–20  $\mu\text{m}$ . Theoretical simulations were performed using a transfer matrix method. Good agreement between experimental and theoretical absorptances was obtained in the full wavelength range of 2–22  $\mu\text{m}$ . Minor discrepancies were attributed to absorptance in the silicon nitride film. Considerations regarding further optimizations of the absorbers are presented.

## 1. Introduction

Infrared (IR) technology has been rapidly expanding over the past few years with great emphasis on detector arrays, including large, high-resolution ( $>128 \times 128$  picture elements) focal plane arrays (FPA). Arrays based on *thermal detectors* have evolved as viable candidates for thermal imaging applications.<sup>(1,2)</sup> The operation of thermal detectors depends on a two-step mechanism. The absorptance of radiation raises the temperature of the device, which in turn changes some temperature-dependent parameter such as electrical conductivity. In order to obtain large temperature changes, the detector structure should be thermally insulated from the surroundings. This can be achieved by fabricating thin membrane structures by means of micromachining. Temperature changes are measured by temperature detectors integrated in the membranes. Temperature detection methods may involve the use of thermopile<sup>(3)</sup> (Seebeck effect), resistive<sup>(2)</sup> or dielectric bolometer,<sup>(4)</sup> pn- or Schottky diode, pyroelectric<sup>(4)</sup> or Golay cell (thermopneumatic). Characteristic features of thermal detectors have the advantage of room temperature operation and the drawbacks of low sensitivity (signal-to-noise ratio) and slow response. For FPAs, however, where the modulation bandwidth is low, these drawbacks become less serious. In order to optimize sensitivity and speed, high absorptance has to be achieved with a low thermal mass (heat capacity).

The aim of this study is to find out if an absorber with a low thermal mass and high absorptance can be fabricated, and to compare the experimental results with the simulated ones.

## 2. Theoretical Considerations

The spectral absorptance  $A(\lambda)$  is defined as the ratio of the absorbed power to the incident optical power. A commonly used measure of performance for the signal-to-noise ratio of an IR detector is the temperature resolution or the noise equivalent temperature difference,  $NETD$ , which can be expressed as,

$$NETD = \frac{4 f^2 \cdot u_N}{C \cdot \tau_{opt} \cdot A_d \int R_V(\lambda) M(\lambda \cdot T_b) d\lambda} \quad (1)$$

where  $R_V(\lambda)$  is the spectral voltage responsivity,  $u_N$  the noise voltage of the detector element and  $A_d$  the pixel unit cell area.  $f$  and  $\tau_{opt}$  are the  $f$ -number and average optical transmission of the camera optics, respectively.  $M(\lambda, T_b)$  is the spectral radiant exitance of a blackbody (optical power per emitting surface area and unit wavelength), where  $\lambda$  is the wavelength,  $T_b$  is the blackbody temperature, and  $C$  is the thermal contrast =  $\partial M/M \partial T$ . According to Planck, one has

$$M(\lambda, T_b) = \frac{2 \pi c^2 h}{\lambda^5 \left[ \exp\left(\frac{hc}{\lambda k T_b}\right) - 1 \right]} \quad (2)$$

The voltage responsivity can be written as

$$R_V(\lambda) = A(\lambda) \cdot F \cdot S \cdot \frac{R_{th}}{\sqrt{1 + \omega^2 \tau_{th}^2}} \approx A(\lambda) \cdot F \cdot S \cdot R_{th}, \quad (3)$$

where  $F$  is the fill factor,  $S$  the transfer function of the temperature-sensitive material or structure (= output voltage per temperature change),  $R_{th}$  the thermal resistance of the membrane used for thermal insulation,  $\omega$  the angular frequency, and  $\tau_{th}$  the thermal time constant. The rightmost term of eq. (3) is valid for frequencies  $\omega \ll 1/\tau_{th}$ .

Evidently, the largest possible absorptance is crucial for obtaining a high responsivity and a small *NETD*. In addition, the thermal resistance needs to be high. Considering the speed of the detector, its time constant is ultimately limited by the thermal time constant, which depends on the thermal mass according to

$$t_{th} = R_{th} C_{th}. \quad (4)$$

A high-speed detector evidently requires a low thermal mass or heat capacity  $C_{th}$ .

Conventional absorbers suffer from either a high thermal mass, *e.g.*, porous films (such as black gold)<sup>(5)</sup> or a relatively low absorptance, *e.g.*, thin resistive metal films.<sup>(6)</sup> However, the most promising absorber today is an interferometric structure, IS,<sup>(7, 8, 9)</sup> as shown in Fig. 1(a). In an ideal case, when the metal film at the bottom reflects all the incident radiation, the optical thickness of the dielectric medium is  $\lambda/4$  and the thin resistive absorbing film at the top has a sheet resistance close to 377  $\Omega$ /square (the vacuum characteristic impedance), 100% absorptance is obtained at the wavelength  $\lambda$ . An IS can provide high absorptance with freedom to tailor the specified wavelength range by using the proper optical thickness of the dielectric medium. The parameter of primary interest is not the spectral absorptance but the integrated absorptance in the 8–12  $\mu\text{m}$  wavelength region,  $A_{8-12}$ , defined as

$$A_{8-12} = \frac{\int_8^{12} A(\lambda) M(\lambda, T_b) d\lambda}{\int_8^{12} M(\lambda, T_b) d\lambda}. \quad (5)$$

Figure 2 shows the spectral absorptance for two ISs with different refractive indices of the dielectric medium which have been optimized for  $\lambda = 10 \mu\text{m}$ . According to Fig. 2, the bandwidth of the absorptance depends on the refractive index of the dielectric medium, which influences  $A_{8-12}$ . From the figure it can be seen that a low refractive index is desirable for obtaining a high optical bandwidth, however, this also implies a thicker dielectric medium, which increases the thermal mass if a constant heat capacity per unit volume  $\sigma$  is assumed.

From this it is clear that if the dielectric medium could be replaced with an air gap whose refractive index  $n_{air} = 1$  and heat capacity  $\sigma_{vac} \cong 0$ ,  $A_{8-12}$  is maximized while  $C_{th}$  is

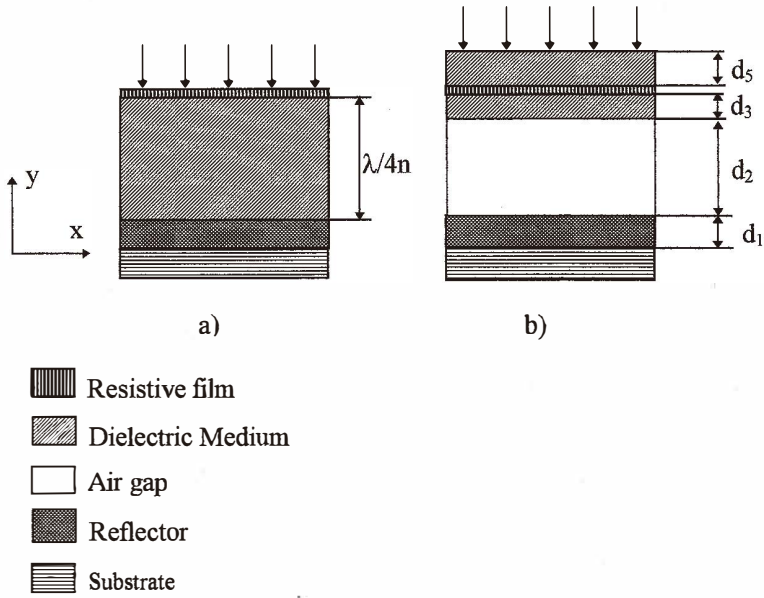


Fig. 1. Scheme of the absorptance structure for: (a) the interferometric structure (IS) and (b) the modified interferometric structure (Mod-IS).

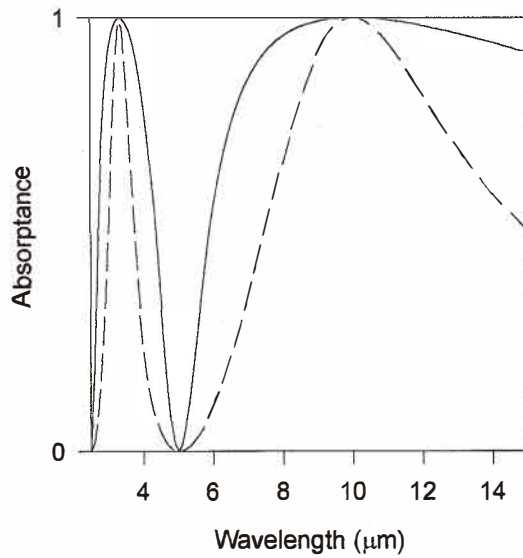


Fig. 2. The absorbance vs. wavelength for two IS absorbers with different refractive indices,  $n$ , of the dielectric medium: solid curve:  $n = 1$  (air gap), and dashed curve:  $n = 3.4$  (silicon).

minimized. Such a structure cannot be fabricated since the thin resistive absorbing film, which has a thickness of about 100 Å, must be supported by another film. A possible structure is a modified IS, Mod-IS, as can be seen in Fig. 1(b). Here the dielectric medium has been replaced with an air gap and the thin resistive absorbing film is supported by a dielectric film which is either on one side or, alternatively, totally embedded in the dielectric medium.

In order to characterize the Mod-IS, complete thermal detector devices with Mod-IS absorbers could be fabricated and the absorptance could be derived from the spectral responsivity of the detector. However, in this case, problems due to low signal-to-noise ratio are likely to occur since the optical power is low in a spectral measurement using a monochromator. Instead, in order to simplify both fabrication and characterization, we have chosen to fabricate absorber structures extending over a large area of the wafer, whose absorptance is easily obtained from FTIR (Fourier transform infrared) spectroscopy.

The aim of this study is to determine if Mod-IS of high absorptance can be fabricated, as well as to compare experimental results with simulated ones. These are necessary steps prior to the final optimization of the structure. The optimized Mod-IS will then be discussed.

### 3. Materials and Experimental Method

Surface micromachining<sup>(10, 11)</sup> is the method of choice when fabricating an absorber structure of the Mod-IS type shown in Fig. 1 (b). The structure consists of, from bottom to top: i) a reflector consisting of a silicon substrate covered with 200 nm gold, ii) an air (or vacuum) gap, iii) a bottom dielectric layer, iv) a resistive metal film of sheet resistance  $R_s$ , and v) a top dielectric layer. The radiation enters from the top. Three different Mod-ISs, denoted A, B and C, were fabricated (see Table 1 for layer thicknesses and Fig. 1 (b) for the layer notation). The structures differ mainly in their layer thicknesses and in the presence or absence of the bottom dielectric layer. In structures B and C, the metal film is embedded in the dielectric medium. This has the advantage of protecting the metal during the removal of the sacrificial layer.

Surface micromachining involves the deposition and patterning of a sacrificial layer

Table 1

Structure parameters of the absorber structures A, B, C of the Mod-IS type. The layer widths are indicated by  $d$  and the sheet resistance of the resistive metal layer by  $R_s$ .

Sample	Fill factor [%]	$d_2 \pm \Delta d_2$ [ $\mu\text{m}$ ]	$d_3$ [ $\mu\text{m}$ ]	$d_5$ [ $\mu\text{m}$ ]	$R_s$ [ $\Omega/\text{square}$ ]
A	90	$2.8 \pm 0.5$	0	0.34	338
B	90	$2.6 \pm 0.5$	0.061	0.34	359
C	70	$2.5 \pm 0.5$	0.34	0.11	368

onto which a membrane material is subsequently deposited. When the membrane material has been patterned the sacrificial layer is removed by etching and the membrane is left hanging free, supported only by its legs or pillars. The fill factor, which is defined as the ratio of the absorbing area to the total area of the structure, will be reduced by: i) the region close to the support pillars as well, as ii) by the area needed for etch holes which are utilized for removing the sacrificial layer. Our designs permit a fill factor of between 70 and 90%. The total area covered by the structure was about  $20 \times 20$  mm. Figure 3 (a) displays a scanning electron micrograph of the absorber structure seen from above and Fig. 3 (b) shows the cross section of the absorber structure. The distance between the pillars is  $100 \mu\text{m}$  and their diameter is  $20 \mu\text{m}$ .

The etching selectivity between the membrane and the sacrificial layer and the stress in the membrane material are important factors to consider when choosing the materials for this structure. If the etching selectivity is poor, undesired etching of the membrane

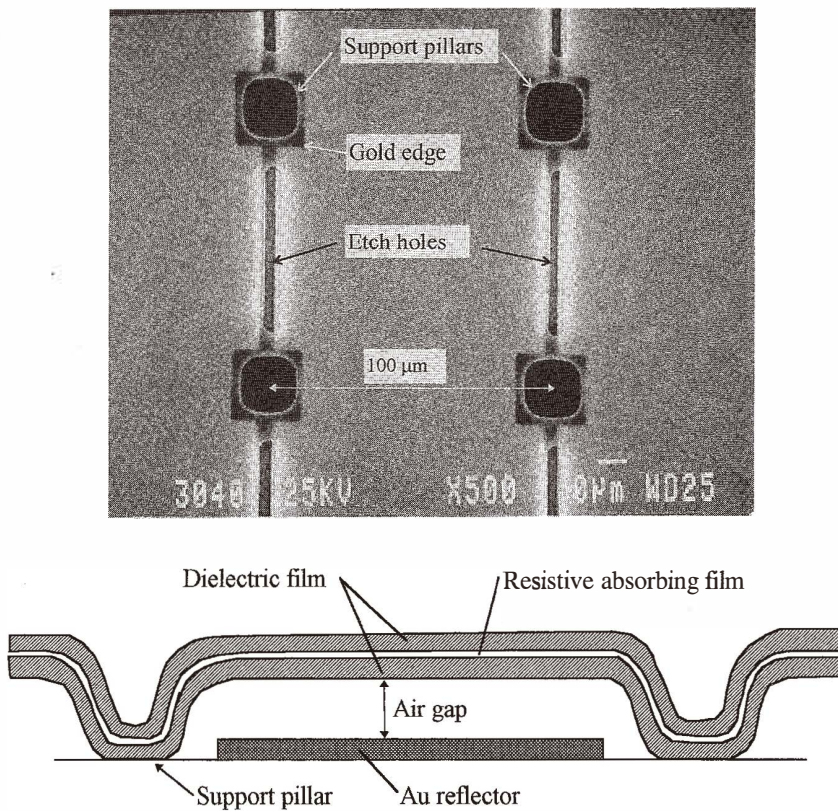


Fig. 3. (a) Scanning electron micrograph of sample structure A seen from the top and, (b) schematic diagram of the cross section (not drawn to scale).

material will occur during the removal of the sacrificial layer. It is also desirable to remove the sacrificial layer with a dry etch, since a wet etch can cause the membrane to stick to the surface of the reflector. If the stress in the membrane film is too high the membrane either breaks or deflects. If the membrane is deflected towards the reflector, the air gap will decrease and, hence, the absorptance characteristics change. Since the Mod-IS will be implemented as an integral part of a microbolometer, the fabrication has to be carried out at temperatures  $< 400^{\circ}\text{C}$  to be compatible with CMOS electronics. This temperature limit has to be taken into account when choosing materials.

There are four different materials that must be chosen when fabricating a Mod-IS: i) the reflector material, ii) the sacrificial layer, iii) the dielectric film, and iv) the resistive film.

i) The reflector material could be made from many types of high-conductivity metal films. It should provide high reflection in the wavelength range of  $8\text{--}12\ \mu\text{m}$  and it should be compatible with the sacrificial layer that is deposited on its surface. We used gold for the reflector, which satisfies these requirements. Gold is easy to deposit and pattern by means of evaporation combined with lift-off techniques. The poor adhesion of gold is improved by depositing a thin film of chromium first.

ii) The sacrificial layer must be easy to remove during the last processing step. The important parameter is the etching selectivity between the sacrificial layer and the other materials. Since its thickness will influence the absorptance behavior, the deposition must be done in such a way that the thickness can be reproduced. We used a spin-deposited polyimide (PI) film as a sacrificial layer. As an organic material, PI is easily removed in an oxygen plasma without affecting the other films. This is necessary since about 5 hours of etching is required to etch about  $50\ \mu\text{m}$  under the membrane. In order to avoid sharp corners where high stress can be concentrated and deflect the membrane, a sloped profile of the sacrificial layer is desirable. A sloped profile of the PI can be obtained using different patterning techniques.<sup>(11)</sup> Since the PI is spin-deposited, the thickness cannot be controlled with high accuracy, in contrast to the possibilities of using, for example, gas-phase deposition techniques.

iii) As a membrane material, silicon nitride ( $\text{SiN}_x$ ) was used. The  $\text{SiN}_x$  ( $x \approx 1.3$ ) films we are deposited using a Vacutec plasma-enhanced chemical vapor deposition (PECVD) system at  $300^{\circ}\text{C}$  and 600 mTorr. Such films exhibit low stress, which is the most important parameter of the membrane material. The measured value of stress was 65 MPa, derived from the change of curvature of a 4" Si wafer before and after deposition. The refractive index as found from ellipsometry at a HeNe laser wavelength of 633 nm was 2.00, which indicated a film of proper stoichiometry.

iv) The absorption takes place in a resistive film where the sheet resistance  $R_s$  is an important parameter.  $R_s$  should be in the range of  $300\text{--}400\ \Omega/\text{square}$  which means that in the case of high-conductivity metals the thickness is  $< 5\ \text{nm}$ . The reproducibility is improved by using materials with higher resistivity, i.e., in the range of  $100\text{--}300\ \mu\Omega\ \text{cm}$ . We chose  $\text{MoSi}_2$  which is sputter-deposited at  $100^{\circ}\text{C}$  using a  $\text{MoSi}_2$  target and subsequently annealed at  $400^{\circ}\text{C}$  to obtain a more stable sheet resistance during the last steps of processing.  $R_s$  was shown to decrease by about 10% during this heat treatment. The sheet resistance of the  $\text{MoSi}_2$  films was measured using a Prometrix Omnimap RS30 four-point probe.

The various absorber structures were characterized by measuring the reflectance using an FTIR instrument fitted with an accessory for specular reflection. A limitation of the instrument is that the reflectance cannot be obtained at normal incidence. Instead, the measurements have been performed at an angle of incidence of  $30^\circ$ . It should be mentioned that there is only a slight dependence of absorptance on the angle of incidence for angles up to about  $30^\circ$ . This angle interval corresponds to the angles covered for the optics  $f=1$ . A silicon chip covered with a 200-nm-thick layer of gold was used as a reference sample.

A separate test structure for the characterization of the optical properties of silicon nitride was fabricated as follows: i) 200 nm of gold was deposited onto a silicon chip, and then ii)  $0.33 \mu\text{m}$  of silicon nitride was deposited using a Vacutec PECVD system. The samples were characterized by FTIR with the specular reflection accessory. A silicon chip covered with a 200-nm-thick gold layer was used as a reference sample.

#### 4. Results and Discussion

The reflectance  $R$  was measured by FTIR for samples A, B and C. The absorptance was obtained from  $A = 1 - R$ . The results of the measurements are shown in Figs. 4 (a), (b) and (c). An absorptance minimum near  $5 \mu\text{m}$  and a broad maximum around  $10\text{--}14 \mu\text{m}$  are noteworthy characteristics of the interferometric structure. This is the expected behavior if

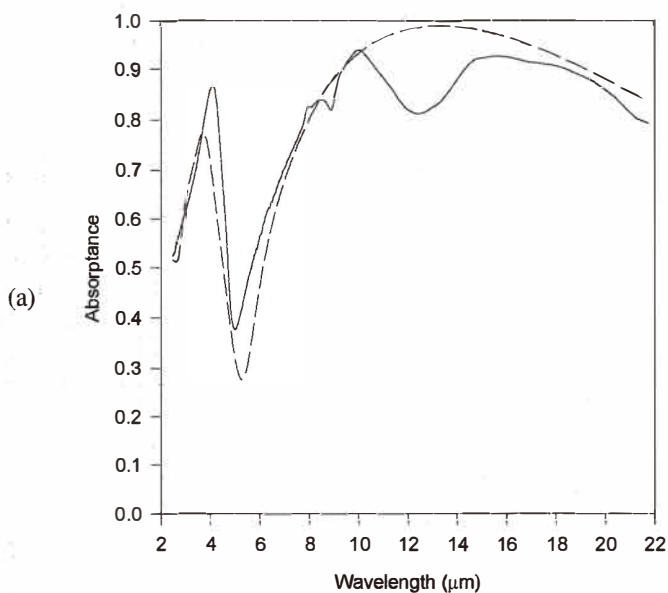


Fig. 4. (a) The reflectance as recorded from FTIR vs. wavelength for sample A: experimental results (solid curves), and simulated (dashed curves).

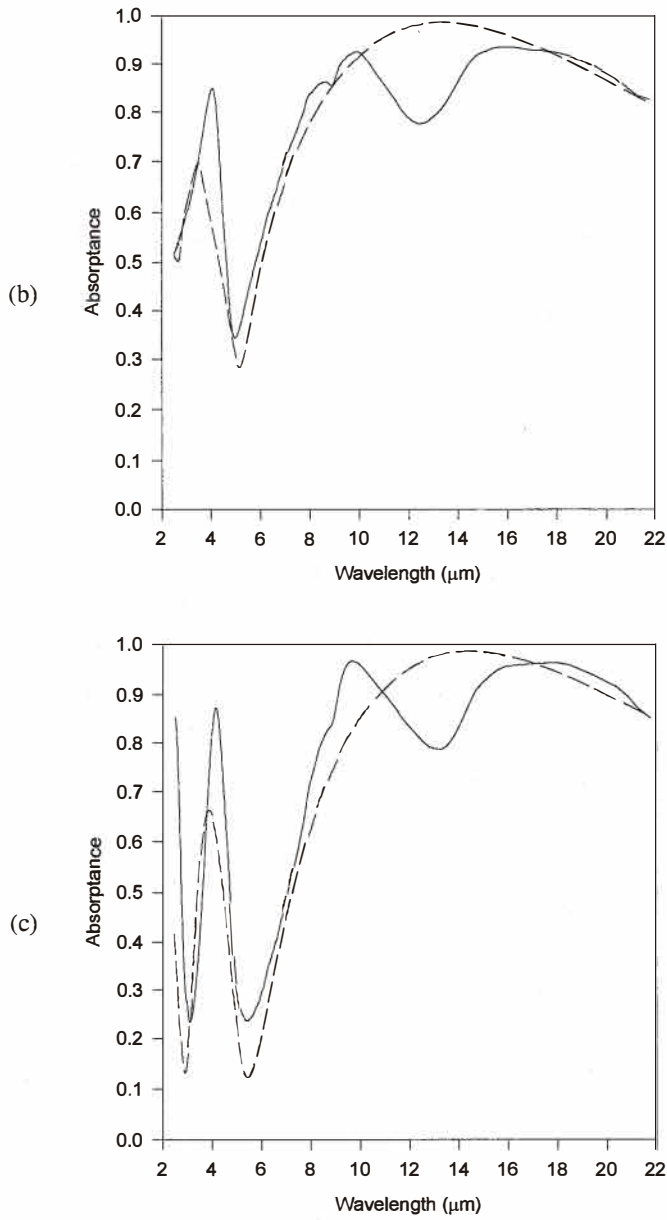


Fig. 4. The reflectance as recorded from FTIR vs. wavelength for sample B (b) and C (c): experimental results (solid curves), and simulated (dashed curves).

the air gap distance is close to  $2.5 \mu\text{m}$ , corresponding to about a quarter wavelength. The air gap distance was somewhat difficult to control due to: i) thickness variations of the spin-deposited polyimide used as a sacrificial layer, and ii) stresses in the membrane material resulting in distortions. It was therefore necessary to measure the thickness after the fabrication of the absorber structures. Two separate methods were used and their results compared: a) direct measurements using scanning electron microscopy (SEM), and b) spectral measurements by FTIR.

a) A SEM image of the cross section clearly showed that the air gap distance  $d_2$  was not constant but varied slightly from the average value, especially in the region close to the support pillars where the membrane was deformed due to stress. The SEM image gave an average  $d_2 = 2.9 \mu\text{m}$ .

b) In order to extract the air gap distance  $d_2$  from the FTIR spectra, it is convenient to separately simulate such spectra using different values of  $d_2$  and compare them with experimentally obtained values. Therefore, a simulation procedure based on a transfer matrix method was developed. As input, the layer sequence, with all the constituent layer refractive indices and thicknesses, and the angle of incidence are given. The method is described below in detail. It was tentatively assumed that the silicon nitride could be modeled with a refractive index of 2.0 over the whole wavelength range, equal to the value found from ellipsometry at 633 nm. This is approximately true for wavelengths  $< 7 \mu\text{m}$  in which the silicon nitride shows no substantial absorptance. To model the films of gold and  $\text{MoSi}_2$  in the simulations an approximation was used where the propagation constant,  $k$ , is written as,

$$k = \sqrt{\frac{\pi\kappa}{c_0\epsilon_0\lambda_0}}(1 + j), \quad (6)$$

where  $\kappa$  is the electrical conductivity,  $\epsilon_0$  the permittivity of free space and  $c_0$  and  $\lambda_0$  the speed of light and the wavelength, respectively, both in vacuum. From spectral comparison, it was immediately found that the experimental curves were broad as compared to the simulated ones. This was attributed to the variation of the air gap distance, as also observed from SEM micrographs. In order to obtain a fair agreement it was necessary to introduce a distribution of widths  $d_2$ . For simplicity, a rectangular probability distribution was used. Finally, the simulated and experimental spectra were compared. The average  $d_2$  obtained in this way is given in Table 1 together with the half-width of the distribution ( $= \Delta d_2$ ). The FTIR spectra of the sample together with simulated and broadened curves are displayed in Figs. 4 (a), (b) and (c). The FTIR spectra have also been compensated for the fill factor not being unity. This compensation assumed 100% transmittance in the area where there was no gold film, i.e., the support pillars and etch holes.

It was found that methods a) and b) above gave nearly the same air gap distance (2.9 as compared to  $2.8 \mu\text{m}$ ). This confirmed the hypothesis that the discrepancy between the value of absorptance predicted for an ideal absorber and the experimental result depended on the air gap distance varying in the lateral direction. Also, at larger wavelengths ( $> 7 \mu\text{m}$ ) differences are observed, in particular, an absorptance minimum is observed in the

wavelength interval of 10–14  $\mu\text{m}$ . This is attributed to absorptance in the silicon nitride, which has also been verified by measurements at SOPRA, France, where a spectroscopic IR ellipsometer was used to measure the complex refractive index of the silicon nitride film.

In order to estimate the extent of absorptance in the silicon nitride, such films deposited onto gold were studied by FTIR. The result is presented in Fig. 5 for a film thickness of 0.33  $\mu\text{m}$ . The angle of incidence was  $30^\circ$  (the same as in the studies of the Mod-IS absorbers). The two sharp peaks at 3.0 and 4.6  $\mu\text{m}$  are due to hydrogen in the film, i.e., N-H and Si-H stretching vibrations, respectively. The dip at 4.2  $\mu\text{m}$  is due to carbon dioxide, whereas the noisy region around 6.5  $\mu\text{m}$  results from water vapor. The silicon nitride exhibits large absorptance due to vibration of the Si-O bonds caused by oxygen contamination, as well as Si-N bonds in the region above 7.5–8  $\mu\text{m}$ . At 12  $\mu\text{m}$  the reflectance exhibits a minimum of 90% and, thus, 10% is absorbed in the film. This minimum coincides with the absorptance minimum observed in the spectra from the Mod-IS absorbers.

The simulation method mentioned above made use of a transfer matrix theory. Matrix theories are suitable for modelling wave propagation in multilayer structures in which the optical properties of the medium vary only in one direction (the y-direction, i.e., perpendicularly to the substrate). If the medium is linear, coupling exists only between pairs of plane wave modes connected by reflection in the layer planes. Transfer matrices of the

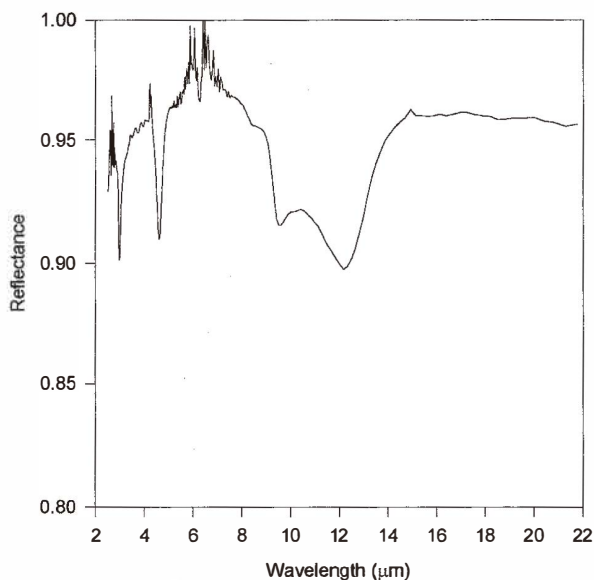


Fig. 5. FTIR spectrum of a silicon nitride film of thickness 0.33  $\mu\text{m}$  deposited by plasma-enhanced CVD onto gold-covered silicon chips. The angle of incidence was  $30^\circ$ .

type dealt with here are of size  $2 \times 2$  and act on two-wave vectors, where  $b_-^s$  and  $b_+^s$  are proportional to the optical field propagating in the  $-y$  and  $+y$  directions, respectively ( $t = \text{transpose}$ ). The index  $s$  denotes all relevant parameters needed for the definition of the plane EM wave: angle of propagation, polarization direction (transverse electric, TE or transverse magnetic, TM), etc. TE (TM) is defined here as having the electric field (magnetic field) parallel to the surface of the substrate. One has

$$\begin{bmatrix} b_-^s \\ b_+^s \end{bmatrix}_k = \begin{bmatrix} T_{11}^s & T_{12}^s \\ T_{21}^s & T_{22}^s \end{bmatrix} \cdot \begin{bmatrix} b_-^s \\ b_+^s \end{bmatrix}_j, \quad (7)$$

where the index  $k$  denotes a location at a larger value of  $y$  than does  $j$ , as is also evident from Fig. 6. Transfer matrices of a layer sequence are obtained by a successive matrix multiplication of the matrices corresponding to single layers or interfaces. One distinguishes between reflection matrices that describe the transfer through an interface, and bulk transfer matrices that model the transfer through a single bulk layer of constant composition. Absorbance is taken care of by using a complex refractive index.

A reflection matrix is written as:

$$R_{kj}^W = \frac{1}{t_{kj}^W} \begin{bmatrix} 1 & r_{kj}^W \\ r_{kj}^W & 1 \end{bmatrix}, \quad (8)$$

where  $W = \text{TE or TM}$ .

The reflection and transmission coefficients are found from Fresnel's laws of reflection.<sup>(12)</sup>

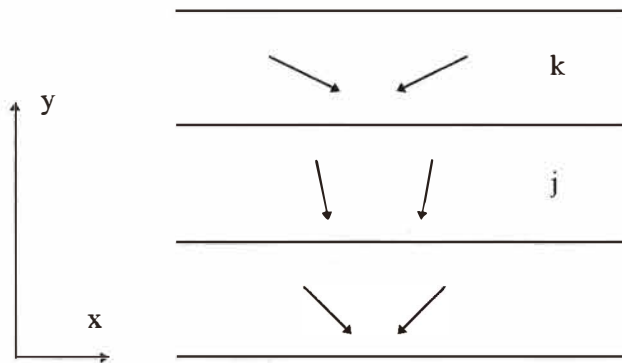


Fig. 6. Scheme of the layer sequence with the electromagnetic wave pattern indicated. The arrows represent plane waves, and their propagation direction is indicated by the direction of the arrow. Plane waves propagating in the  $+y$  direction are not shown for clarity.

The bulk transfer matrix is written as

$$B_j^w = \begin{bmatrix} \exp(-i\Phi_j) & 0 \\ 0 & \exp(-i\Phi_j) \end{bmatrix}, \quad (9)$$

with

$$\Phi_j = n_j \frac{2\pi}{\lambda} d_j \cos \theta_j, \quad (10)$$

where  $n_j$  is the refractive index in layer number  $j$ ,  $\lambda$  the vacuum wavelength, and  $d_j$  the layer thickness. The angle of propagation  $\theta_j$  in layer  $j$  can be found from  $\sin \theta_j = (n_{ref}/n_j) \sin \theta_{ref}$ . The index *ref* denotes a reference layer, *e.g.*, air or vacuum. Finally, the absorptance is calculated from the two-wave vector  $(b_+^s, b_-^s)^t$  in layer No. 6 (see Fig. 1 (b)), according to

$$A = 1 - \frac{|b_+^s|^2}{|b_-^s|^2}. \quad (11)$$

For an angle of incidence other than zero ( $30^\circ$  was used for both the experiments and the simulations),  $A$  is calculated for unpolarized radiation by taking the average of the corresponding TE and TM values.

When optimizing the absorber structures,  $A_{8-12}$  should be as large as possible since this maximizes the optical signal and thus the signal-to-noise ratio. For an ideal structure, that is, assuming negligible absorptance in the dielectric film, values of  $A_{8-12} > 0.95$  may be obtained. However, if the dielectric film possesses absorptive behavior,  $A_{8-12}$  may still become large for properly selected structures. For example, for a specified wavelength, the larger the absorptance in the dielectric film, the larger  $R_s$  is. The latter fact is compatible with a small absorptance in the metal, thus keeping the total absorptance nearly constant. Difficulties are encountered when the absorptance in the dielectric film is strongly wavelength-dependent. In this case, the broadband behavior of the absorptance cannot, in general, be maintained. In order to accurately model the structure, the complex refractive index of the dielectric medium versus wavelength is needed.

For detector arrays it is desirable to achieve a high pixel-to-pixel uniformity with regard to  $A_{8-12}$ . The air gap distance is the parameter which is most prone to variations, due to stresses in the membranes as well as the resulting thickness variations of the sacrificial layer, as discussed above. Changing the air gap distance results in a wavelength shift of the absorptance spectrum which, in turn, has an influence on  $A_{8-12}$ . Since the absorptance peak is very broad (Fig. 2) the relative variation of  $A_{8-12}$  is minor for the case of maximum  $A_{8-12}$ . The two requirements are thus compatible with each other. However, spectral variations of the detector response are known to render the nonuniformity correction difficult and should be avoided if possible.

A complete bolometer device should also include a thermistor layer for temperature detection which must be taken into consideration during the optimization procedure.

## 5. Summary and Conclusions

One of the most essential parts of a thermal IR detector is the absorber, which is expected to provide the detector with high absorptance in the specified wavelength range without adding too much thermal mass. An absorber that satisfies these requirements is an interferometric structure which consists of a reflector, an air gap of thickness approximately equal to a quarter wavelength, a thin resistive absorbing film with a sheet resistance close to  $377 \Omega/\text{square}$  (the vacuum characteristic impedance), and a thin dielectric film needed for mechanical support of the latter.

Such absorbers were fabricated and characterized and their spectra were compared with theoretically simulated spectra. The fabrication was based on surface micromachining with molybdenum silicide as the resistive film material, silicon nitride as the dielectric medium, and gold as the reflector. Polyimide was used as a sacrificial layer during membrane fabrication. The samples were characterized using Fourier transform infrared spectroscopy. After compensation for a nonunity fill factor a mean absorptance of 80–90% was obtained in the very broad wavelength region of 8–20  $\mu\text{m}$ . Theoretical simulations were performed using a transfer matrix method. Good agreement between experimental and theoretical absorptances was obtained in the full wavelength range of 2–22  $\mu\text{m}$ . Minor discrepancies were attributed to absorptance in the silicon nitride film.

Considerations regarding further optimizations of the absorbers were presented.

## References

- 1 P. W. Kruse: *Proceedings of SPIE* **2552** (1995) p. 556.
- 2 R. A. Wood: *Proceedings of SPIE* **2020** (1993) p. 322.
- 3 R. Lenggenhager, H. Baltes and T. Elbel: *Sensors and Actuators A* **37-38** (1990) 216.
- 4 D. E. Witter, H. R. Beratan, B. M. Kulwicki and A. Amin: *TI Technical J.*, Sep. – Oct. 94 (1994) 19.
- 5 W. Lang, K. Kuhl, and H. Sandmaier: *Sensors and Actuators A* **34** (1992) 243.
- 6 W. Woltersdorff: *Z. Phys.* **91** (1934) 230.
- 7 K. C. Liddiard: *Infrared Physics* **34** (1993) 379.
- 8 P. Eriksson, J. Y. Andersson and G. Stemme: *Physica Scripta* **T54** (1994) 165.
- 9 J. J. Monzón and L. L. Sánchez-Soto: *Applied Optics* **33** (1994) 5137.
- 10 R. T. Howe: *J. Vac. Sci. Technol.* **B6** (1988) 1809.
- 11 P. Eriksson, J. Y. Andersson, G. Stemme, G. Hansson and K. Joelsson: *Third international symposium on long wavelength infrared detectors and arrays* (The Electrochemical Soc., NJ, 1995) p. 67
- 12 D. K. Cheng: *Field and wave electromagnetics* (2nd edition, Addison-Wesley 1991) pp. 413 – 415.